Human Movement Sciences
Sport, Exercise & Health (research)

Research Internship Research Master 2013-2014
(Course code B_RIRM)

On the Neural Origin of Muscle Synergies

VU University Amsterdam
Faculty of Human Movement Sciences
Qualification: MSc in Human Movement Sciences
Research internship Research Master

Author: Ingmar Engbert Jacob de Vries

Supervisor(s): Dr. Tjeerd W. Boonstra &
Prof. Dr. Andreas Daffertshofer

September 2014

move research institute amsterdam

Abstract

We modified the degree of muscle synergy, i.e. how much two muscles have to coordinate, and studied the effect of this manipulation on cortico- and intermuscular coherence. 16 healthy subjects performed a visual feedback task in which they controlled a cursor displayed on a monitor by pressing compliant pinch grip force sensors with both hands. The horizontal position of the cursor was determined by the difference between left and right forces. We manipulated the sensitivity of the cursor for this difference, creating three conditions: low, medium, and high synergy level. Cortical activity was measured using a 64-channel EEG system, and muscle activity using 8x8 high-density EMG electrode grids on the FPB muscle of both hands. Following the uncontrolled manifold framework, the degree of muscle synergy was quantified as the ratio R_V between the variability along the dimension that the muscles leave uncontrolled (sum of bimanual forces) and the variability along the dimension that the muscles do control (difference between bimanual forces). We determined this both in time and frequency domain. Cortico- and intermuscular coherences were estimated in terms of EEG-EMG and EMG-EMG coherence, respectively. The manipulation worked as intended, i.e. R_V was highest for the high synergy condition and lowest for the low synergy condition. In the frequency domain, R_V followed a similar pattern in the 0 - 0.5 Hz and for 2+ Hz frequency ranges. For the 0.5 – 2 Hz frequency band this pattern was inverted. The high synergy condition showed highest intermuscular coherence and lowest corticomuscular coherence, the low synergy condition showed the opposite. These results support the idea that corticomuscular and intermuscular coherence reflect two distinct neural pathways. Corticomuscular coherence reflects direct innervation to individual muscles, while intermuscular coherence reflects a diverging pathway that makes coordination between muscles possible (i.e. muscle synergies).

Keywords: Muscle synergy, corticomuscular coherence, intermuscular coherence, functional connectivity

Table of contents

1. Introduction

1.1 The Bernstein Problem

In everyday life, the human motor system is faced with a wide range of possibilities how to successfully perform a specific movement, such as grabbing an object with the hand. That is, there is a large set of possible parameter values (e.g. combinations of joint angles) that can lead to the desired end result (i.e. grabbing the object). The central nervous system (CNS) has to control and coordinate these many degrees of freedom (DOFs) of the neuromuscular system and select a movement trajectory from a range of possible solutions. This redundancy is evident on multiple levels of analysis (e.g. muscle activation and joint kinematics) and imposes a large computational load on the CNS. Bernstein was one of the first to address this apparent "redundancy or DOFs problem" of our nervous system, which is also referred to as "The Bernstein Problem" (Bernstein, 1967; Latash, Scholz, & Schöner, 2007; Tuller, Turvey, & Fitch, 1982; Turvey, Fitch, & Tuller, 1982).

How our nervous system solves this problem is a fundamental question in the field of motor control and many different solutions have been proposed (Latash et al., 2007; Nazarpour, Barnard, & Jackson, 2012). Some researchers propose a reduction of the number of DOFs to lower the computational load on the CNS (Bernstein, 1967; Vereijken, Emmerik, Whiting, & Newell, 1992), while others suggest that the nervous system actually uses this redundancy to optimally achieve the movement goal (Diedrichsen, Shadmehr, & Ivry, 2010; Latash et al., 2007; Scott, 2004; Todorov, 2004). These solutions to the degrees of freedom problem are generally referred to as 'muscle synergies', although models and implementations of these synergies vary across research groups.

1.2 The Concept of Muscle Synergies

Muscle synergies are often described as being imposed by anatomical architecture, thus forming a low-level constraint. According to this interpretation a muscle synergy is a specific pattern of relative levels of muscle activation, imposed at the level of the spinal cord, i.e. as an interneuronal module (Bizzi & Cheung, 2013). These low-level muscle synergies may also result from couplings between muscles at an even lower level of organisation arising from e.g. limb biomechanics (Ting, Chvatal, Safavynia, & Mckay, 2012; Ting & McKay, 2007), but they require additional neural structures to incorporate these biomechanical properties into specific synergies (Bizzi & Cheung, 2013). The central nervous system can flexibly combine these muscle synergies to generate the wide range of movements needed in everyday life. In this way, the computational load for higher centres of the central nervous system is strongly reduced as higher centres only control a small number of variables on the level of the movement task, instead of controlling the large number of parameters in the neuromuscular system (Latash et al., 2007).

An alternative perspective is that rather than reducing the number of DOFs by low-level constraints, the nervous system actually exploits this redundancy to optimize movement performance (Diedrichsen et al., 2010; Latash, Scholz, & Schöner, 2002; Latash et al., 2007; Scott, 2004; Todorov, 2004) or to successfully respond to perturbations (Kelso, 2008). Hence, in this view synergies are not constraints that reduce the number of DOFs, but synergies emerge from high-level control policies to optimize movements (Latash et al., 2007). Evidence for this comes from experiments showing that the central nervous system selectively controls movement variability in the task-relevant dimensions while leaving the remaining dimension uncontrolled (i.e. the uncontrolled manifold (UCM)), thus

effectively buffering variability in task-irrelevant dimensions (Latash et al., 2007; Nazarpour et al., 2012). Moreover, this UCM framework provides an experimental approach to quantify and experimentally manipulate muscle synergies. For example, Nazarpour et al. (2012) showed that within a few trials subjects learn to use synergies between arbitrary muscle pairs depending on abstract task demands.

1.3 Implementation of Muscle Synergies in the Central Nervous System

Irrespective of the theoretical perspective, most studies on muscle synergies are based on a functional description of a muscle synergy, i.e. at the level of limb movements and muscle activation. Little is known about how muscle synergies are implemented in the central nervous system and most physiological mechanisms remain speculative. Bizzi & Cheung (2013) suggest it is important to distinguish between phylogenetically older and newer descending motor systems. The older system contains (diverging) descending efferent neurons that innervate spinal interneurons and activate spinal modules, whereas the newer system involves direct innervations of spinal motoneurons of individual upper limb muscles to further sculpt activations of specific muscles. Although these pathways can only be measured directly using invasive recording techniques, the effect of direct corticospinal projections can be assessed using corticomuscular coherence* (Baker, Olivier, & Lemon, 1997; van Wijk, Beek, & Daffertshofer, 2012). Likewise, the diverging projections of the older pathways may be captured by intermuscular coherence, since they would result in common oscillatory input to distinct muscles (Boonstra & Breakspear, 2012; Boonstra, Daffertshofer, et al., 2009; Farina, Negro, & Jiang, 2013).

Although there is ample evidence that corticomuscular coherence reflects direct corticospinal projections (van Wijk et al., 2012), the suggestion that intermuscular coherence specifically captures older motor systems with more diffuse projections remains speculative. Experimental results suggest that corticomuscular and intermuscular coherence represent different descending pathways (Boonstra, van Wijk, Praamstra, & Daffertshofer, 2009). They found intermuscular coherence between bilateral homologous hand muscles when the subjects were asked to stabilize force output and corticomuscular coherence during constant force output, suggesting task dependence for use of different descending pathways. Intermuscular coherence may specifically capture a common excitatory drive to muscles that work together, i.e. in a synergy (Boonstra, Daffertshofer, et al., 2009). For example, two extrinsic hand muscles whose activities were tightly coupled for a precision grip task showed intermuscular coherence, implying that here descending pathways diverge to control the two muscles as a single unit (Fuglevand, 2011). Similarly, Nazarpour et al. (2012) found intermuscular coherence between two ipsilateral hand muscles synergistic in precision grip and they found a task-dependent modulation of this coherence, i.e. intermuscular coherence was significantly higher when the task required higher coordination between the muscles.

In this study we test the relationship between bilateral muscle synergies and intermuscular and corticomuscular coherence, by experimentally manipulating the degree of muscle synergy. When a relatively stronger synergy is required (muscles have to coordinate) we expect to find higher levels of intermuscular coherence and lower levels of corticomuscular coherence reflecting a larger contribution from diverging projections in phylogenetically older motor systems. In contrast, when a relatively weaker synergy is required and muscles can be controlled separately, we expect higher

*Coherence quantifies the coupling between two signals (Bruns, 2004). For corticomuscular coherence that is between EEG/MEG and EMG, for intermuscular coherence that is between EMG and EMG of different muscles.

levels of corticomuscular coherence and lower levels of intermuscular coherence reflecting a larger contribution from direct corticospinal pathways. This result would mean that our nervous system can flexibly regulate the contribution of muscle synergies depending on task demands and that those muscle synergies can be assessed with intermuscular coherence.

2. Materials and Methods

2.1 Subjects

Sixteen healthy right-handed subjects (8 female, age = 25.5 ± 4.3) volunteered in the study. The local ethics committee at the Faculty of Human Movement Sciences, VU University Amsterdam approved the experimental protocol and prior to the recordings each subject provided written informed consent.

2.2 Experimental Protocol

Subjects performed a bimanual task in which the degree of synergy between homologous hand muscles was experimentally manipulated, while we assessed intermuscular and corticomuscular coherence.

Subjects were instructed to control a cursor displayed on a computer monitor in front of them by generating bimanual force by pressing a compliant force sensor using a pinch grip with each hand (Fig. 1A and B).

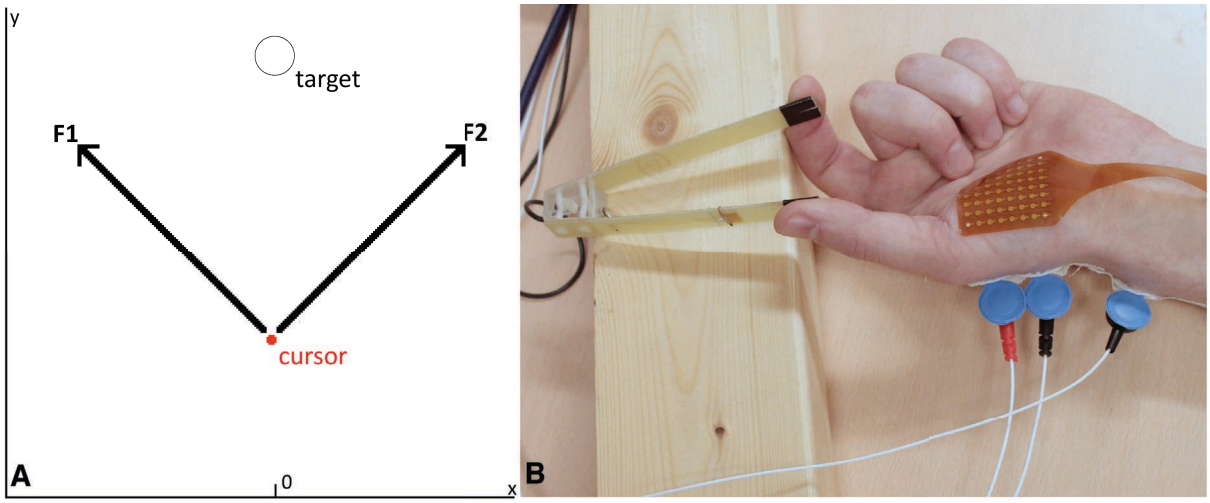

Figure 1. Setup and Protocol. A) Force level projection. Cursor and target are the visual feedback displayed on the monitor. **B)** Custom made compliant pinch grip force sensor and high density electrode grid on Flexor Pollicis Brevis.

The position of the cursor is determined by a linear weighting of the two forces:

$$\begin{pmatrix} x \\ y \end{pmatrix} = \begin{pmatrix} c11 & c12 \\ c21 & c22 \end{pmatrix} * \begin{pmatrix} F_l \\ F_r \end{pmatrix}$$

where x and y are the screen coordinates and F_l and F_r are the force levels generated by the left and right hand, respectively (Fig. 1A). The 2x2 projection matrix c converts the generated force levels to screen coordinates. The cursor moves up when force is applied to both sensors and stays in the starting position when no force is applied (red dot in Fig. 1A).

The required level of bilateral muscle synergy was experimentally manipulated by changing the projection matrix c (Nazarpour et al., 2012). For example, when

$$c = \begin{pmatrix} -10 & 10 \\ 1 & 1 \end{pmatrix}$$

the x-position of the cursor is relatively sensitive to differences between the two force levels so a relatively strong synergy between the two hands is required to perform the task successfully (i.e. get the cursor in the circular target). That is, even a small difference between F_l and F_r will move the cursor sideways. In contrast, when

$$c = \begin{pmatrix} -0.01 & 0.01 \\ 1 & 1 \end{pmatrix}$$

the x-position of the cursor is relatively insensitive to differences between the two force levels, i.e. a relatively weak synergy between the two hands is required. For the latter case, the total force needs to be controlled to move the cursor up or down, but a large variability in the ratio of the two force levels is tolerated (bilateral forces are allowed to differ). Nazarpour and co-workers showed in a similar experiment that when imposing such a task-relevant dimension within cursor space, subjects automatically buffer their movement variability in the task-irrelevant dimension within a few trials (Nazarpour et al., 2012).

Subjects were instructed to track a visual target by moving the cursor on the monitor. At the start of a trial, the target was in the starting position (see cursor in Fig. 1A). During the first 5 s of a trial, the target moved linearly to the final target position (force ramp), where it stayed for the remaining 10 s of the trial (constant force). The inter-trial interval was 5 s during which the performance score was presented (percentage of time the cursor was in the target). After the rest period the target automatically reappeared at the starting position and a new trial started. Figure 2 shows an example of a single trial. The duration of a single trial was 20 s.

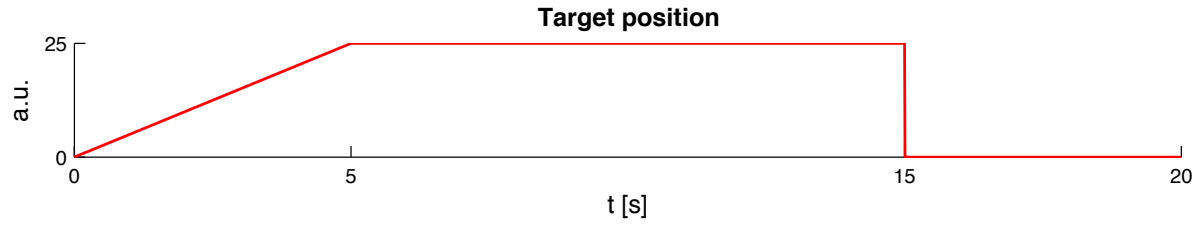

Figure 2. Target position. Single trial time series of vertical target position in arbitrary units (a.u.).

The required level of bilateral synergy was experimentally varied in three conditions (low, medium, high) by varying the projection matrix c:

$$c1 = \begin{pmatrix} -0.01 & 0.01 \\ 1 & 1 \end{pmatrix}$$

$$c2 = \begin{pmatrix} -0.33 & 0.33 \\ 1 & 1 \end{pmatrix}$$

$$c3 = \begin{pmatrix} -10 & 10 \\ 1 & 1 \end{pmatrix}$$

Each projection matrix was used in a block of 20 trials, i.e. the duration of a block was 400 s or about 7 minutes. In addition to the required level of synergy, the total force level was varied to prevent participants from learning the exact force level and to ensure that they were dependent on visual feedback for successful task performance. The force level necessary during the constant force part varied between two levels (1.7 N and 2.1 N per hand) and trials with different force levels were randomized within a block. The order of the 3 blocks was counterbalanced between subjects. Between the blocks there was a two-minute break. Participants were motivated to perform the task as good as possible (i.e. follow the target with the cursor) by promising a price for the participant with the best average performance.

2.3 Data Acquisition

Corticomuscular coherence (CMC) and intermuscular coherence (IMC) were assessed using electroencephalography (EEG) and high-density surface electromyography (HDsEMG). EEG was recorded using a 64-electrode nylon cap placing the electrodes according to the extended 10-20 system and amplified using a 64-channel Refa amplifier (TMSi, Enschede, The Netherlands; sample rate 1024 Hz). HDsEMG was recorded using two 64-channel (8x8, IED 4 mm) electrode grids (Fig. 1B) and amplified using a 128-channel Refa amplifier (TMSi, Enschede, The Netherlands; sample rate 2048 Hz). The grids were placed over the flexor pollicis brevis (FPB) muscle of both hands. Pinch grip force was recorded using a custom-made force sensor (Boonstra et al., 2005) (Fig. 1B) and amplified using a National Instruments amplifier (NI SCXI-1121, sample rate 1000 Hz). At the start of each trial, the force sensor amplifier sent a synchronization pulse to both Refa amplifiers, which was used to align data offline.

2.4 Preprocessing

The data analysis was performed in Matlab (2012a, The MathWorks, Natwick, MA, USA) using the Fieldtrip toolbox for EEG/MEG-analysis (http://www.ru.nl/neuroimaging/fieldtrip; Oostenveld, Fries, Maris, & Schoffelen, 2011). The EMG, EEG and force signals were aligned using the aforementioned synchronization pulse and segmented into separate trials.

Force signals were linearly interpolated to 2048 Hz. Only the constant force part of each trial was selected to asses bilateral muscle synergies, i.e. from t=6 to t=15 s (excluding the first second of constant force to avoid transient activity).

EEG signals were linearly interpolated to 2048 Hz and high-pass filtered (Butterworth, second order, cut off 1 Hz). The signals were band-stop filtered at 50 Hz and its higher harmonics to remove line noise. ICA was used to remove eye-blinks, eye-movements and muscle activity from the EEG data (Jung et al., 2000).

Bad HDsEMG channels were removed and on average 59±4 channels per hand were used for further analysis. The HDsEMG signals were re-referenced to the reference electrode (placed on the process styloid of the radius), high-pass filtered (Butterworth, second order, cut off 10 Hz) and band-stop filtered at 50 Hz and its higher harmonics to remove line noise. Principal component analysis was applied to the HDsEMG signals to reduce the effects of amplitude cancellation and of heterogeneity in the motor unit action potentials (Staudenmann, Kingma, Daffertshofer, Stegeman, & van Dieën, 2006; van de Steeg, Daffertshofer, Stegeman, & Boonstra, 2014). After removing the leading

components the signals were rectified via the analytical signal constructed using the Hilbert transform. This provides an instantaneous amplitude estimate of the EMG signal, which reflects the net input to the motor unit pool. Rectification is preferred when assessing common input between EMG signals at low force levels (Boonstra & Breakspear, 2012; Farina et al., 2013; Myers et al., 2003). Rectified EMG signals were averaged across all grid electrodes for each hand separately (van de Steeg et al., 2014) .

2.5 Data Analysis

2.5.1 Muscle Synergies

Muscle synergies can be quantified according to the UCM method as

$$R_V = \frac{V_{UCM}}{V_{ORT}} \quad \textbf{(1)}$$

Where V_{UCM} is the variability in the dimension irrelevant for task success (i.e. the uncontrolled manifold) and V_{ORT} the variability in the dimension orthogonal to the UCM, i.e. the dimension relevant for task success (Latash et al., 2002, 2007). Strictly we don't have a completely uncontrolled manifold here, since subjects have to control both DOFs in the task parameters (x- and y-position of cursor). Nevertheless, we manipulate the degree with which both DOFs need to be controlled (Nazarpour et al., 2012) and use the UCM method here to quantify the changes in bimanual coordination.

Here we use the variance within a trial as measure of movement variability (Scholz, Kang, Patterson, & Latash, 2003). This approach is preferable when the number of trials is small. Movement error was computed by subtracting the target forces from the measured force signals. To obtain fluctuations in the UCM and ORT dimensions the error signal was then rotated by 90 degrees. That is, in this experimental setup the ORT and UCM dimensions represent the difference and the sum of the two forces, respectively. In this experiment the difference of the two forces is the manipulated performance variable and hence is considered the ORT dimension, i.e. the controlled manifold.

The variances V_{UCM} and V_{ORT} were calculated within each trial. The ratio of these variances gives the quantitative measure of synergy (R_V) according to equation (1). When $R_V < 1$ this indicates no synergy is present, whereas $R_V > 1$ indicates a synergy between bilateral hand muscles (Latash et al., 2007). To correct for the inherent skewness of ratio data, the R_V values were log transformed before averaging to project the data on the interval of $[-\infty, \infty]$, where $R_V > 0$ indicates a synergy and $R_V < 0$ no synergy (Verrel, 2010). The R_V values were then averaged over the 10 trials of each condition.

Previous studies have generally investigated the measure of synergy R_V in the time domain (Latash et al., 2007). To investigate the time scale at which the bilateral synergy is established and investigate the potential relationships with CMC and IMC, we here extend the measure of synergy R_V to the frequency domain. Indeed, Scholz et al. (2003) already showed that there seem to be different time scales involved in the structure of the variability. The power spectral density (PSD) describes the distribution of the variance over frequency, such that the integral of the PSD across frequencies is equal to variance of a signal. Hence equivalent to equation (1) the measure of synergy R_V in the frequency domain is given by:

$$R_v(f) = \frac{P_{UCM}(f)}{P_{ORT}(f)} \quad \textbf{(2)}$$

where $P_{UCM}(f)$ and $P_{ORT}(f)$ are the PSD in the UCM dimension and the ORT dimension, respectively. The PSD over the whole trial length was calculated using a multi-taper method based on discrete prolate spheroidal sequences (Slepian sequences) as tapers (Mitra & Pesaran, 1999), i.e. the data was multiplied by several orthogonal tapers and Fourier-transformed:

$$X_k(f) = \sum_{t=1}^{N} w_t(k) * x_t * e^{-2\pi i f t} \quad \textbf{(3)}$$

where X_k is the Fourier Transform of signal x, $w_t(k)$ the k^{th} orthogonal taper, f frequency, t time and N the length of the signal. To get a spectral estimate at a certain frequency of interest, the squared magnitudes of the orthogonally tapered estimates at that frequency are then averaged:

$$S_{MT}(f) = \frac{1}{K}\sum_{k=1}^{K} |X_k(f)|^2 \quad \textbf{(4)}$$

where S_{MT} is the spectral estimate and K the total number of orthogonal tapers (Mitra & Pesaran, 1999). The amount of smoothing trough multi-tapering was set at $\pm$ 0.2 Hz, which means a 0.4 Hz smoothing box was used around each frequency of interest.

The quantification of muscle synergies in equation (2) directly relates to phase synchronization, in that $P_{UCM}(f)$ signifies anti-phase locking and $P_{ORT}(f)$ in-phase locking between F_l and F_r. We hence also investigated the coherence and relative phase between F_l and F_r to facilitate interpretation. Complex coherency was estimated according to Rosenberg and co-workers (Rosenberg, Amjad, Breeze, Brillinger, & Halliday, 1989) as

$$C_{xy}(f) = \frac{P_{xy}(f)}{\sqrt{|P_{xx}(f)||P_{yy}(f)|}} \quad \textbf{(5)}$$

where C_{xy} is the complex valued coherency between signal x and y, (e.g. the two force signals), P_{xx} and P_{yy} the auto-spectra of signal x and y, respectively and P_{xy} the cross-spectrum between signal x and y. The magnitude-squared coherence (MSC) is then given by

$$MSC_{xy}(f) = |C_{xy}(f)|^2 \quad \textbf{(6)}$$

and the relative phase between the two force signals is calculated as the argument of the complex valued coherency.

2.5.2 Cortico- and Intermuscular Coherence

We localized the two sources in the brain showing maximal CMC with left and right hand HDsEMG signals using a beamforming method, DICS (Dynamic Imaging of Coherent Sources) (Gross et al., 2001; Schoffelen, Poort, Oostenveld, & Fries, 2011). Since we did not have access to individual subjects anatomical MRI data, we used the volume conduction model, source model and MRI templates integrated in the Fieldtrip toolbox (Holmes et al., 1998; Oostenveld et al., 2011; Oostenveld, Stegeman, Praamstra, & Oosterom, 2003). Using this method, first the cross-spectral

density (CSD) between all EEG signal pairs and between all EEG signals and the HDsEMG signals was calculated, again using a multi-taper method with a centre frequency of 23 Hz and $\pm$7 Hz of spectral smoothing (sensor level analysis showed significant CMC in the 16-30 Hz range). We used the averaged CSD over the *z*-scored data of all subjects to localize two average sources.

For each of the two locations of maximal CMC we constructed a spatial filter per subject that allowed us to reconstruct virtual source signals. The virtual source signals calculated this way contain a magnitude and a direction and hence yield three signals (in *x*, *y*, and *z* direction) for each solution point. Singular value decomposition was used to select one dimension in the 3D space that explains most variance, thus leaving us with one source signal per subject per hand.

Magnitude squared coherence between the virtual source signals and the averaged HDsEMG signals (CMC) and between the averaged HDsEMG signals of the two hands (IMC) was calculated over the constant force part (t = 6 - 15 s). Again, a multi-taper method was used for spectral decomposition. The amount of smoothing trough multi-tapering was set at $\pm$1.5 Hz, which means a 3 Hz smoothing box was used around each frequency of interest. Based on the grand averages the frequency ranges of interest (showing significant coherence) were selected for statistical analysis.

2.6 Statistics

Statistical analysis was performed in IBM SPSS Statistics Version 21. A 3x2 repeated measures ANOVA with within-subject factors *synergy level* and *force level* was used to test for significant differences in R_V in the time domain between conditions at group level. Likewise, neural coherence values in the frequency bands of interests were compared using the same 3x2 repeated measure ANOVA. Hence four 3x2 repeated measures ANOVA were performed: R_V, CMC between the left hand and it's virtual source signal, CMC between the right hand and it's virtual source signal and IMC between both hands. A 3x1 repeated measures ANOVA with within-subject factor *synergy level* was used for each frequency band of interest to test for significant differences in R_V *(f).* Likewise, coherence values between left and right hand force signals were compared using the same 3x1 repeated measures ANOVA. The 95% confidence intervals of the coherence estimates were determined through phase randomization.

3. Results

3.1 Muscle Synergies

Figure 3 shows force data of a representative participant and demonstrates the effectiveness of the experimental manipulation: In the low synergy condition the two forces were allowed to differ from each other (Fig. 3A and B) and the variability is most prominent in the ORT dimension (Fig. 3C). In contrast, in the high synergy condition the two forces differ relatively little from each other and variability is most prominent in the UCM dimension.

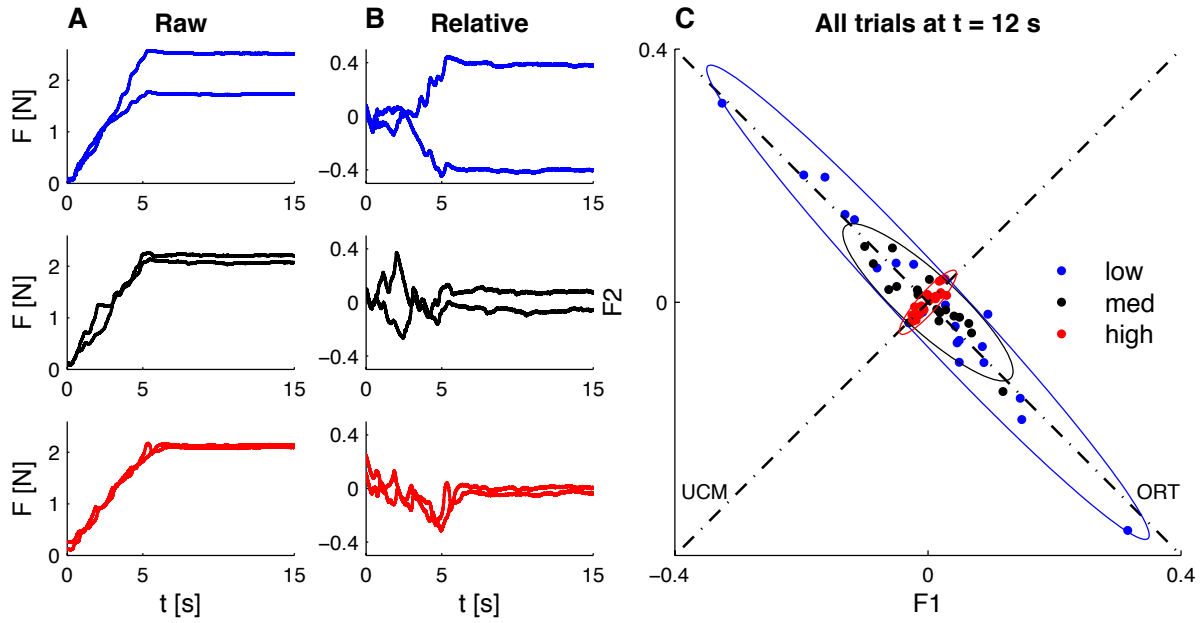

Figure 3. Force data of exemplar participant. The rows show the three synergy levels (Blue = low synergy level, black = medium synergy level, red = high synergy level). **A)** Time series of raw force signals of both hands for three representative trials. **B)** Time series of error signals (force signals relative to target signals). **C)** Cluster plot with on the horizontal and vertical axes force levels of the left and right hand, respectively, at t = 12 s for all 16 participants. Values in panel C are relative to the average over those trials. Ellipses show 95% confidence interval.

R_V is calculated according to equation (1) to quantify the level of synergy for each condition separately. Figure 4 shows the average R_V values for each condition and shows a significant main effect of synergy level (F (2, 30) = 182.36, p < 0.001). No significant main effect of absolute force level or interaction effect was found. $R_V < 0$ and $R_V > 0$ quantify no synergy and synergy, respectively. Hence, this analysis confirms that the conditions differ from each other as intended.

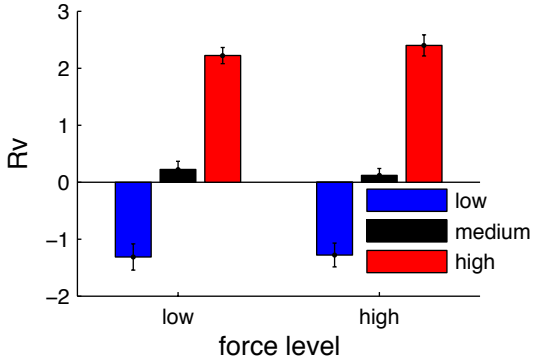

Figure 4. The level of muscle synergy R_V across experimental conditions. Values are averaged over the 10 trials per condition. Blue = low synergy level, black = medium synergy level, red = high synergy level. Bars show the average over participants, error bars show the standard error of the mean.

To investigate the time scale at which the bimanual synergy is established we extended the analysis to the frequency domain. Figure 5 shows the power in both dimensions and R_V as a function of frequency. As expected, most of the power can be seen in the lower frequencies (Fig. 5A and B). For low frequencies (< 0.5Hz) the power in the orthogonal dimension decreases with increasing synergy level (high condition). In contrast, the power in the UCM dimension increases with increasing synergy level. Consequently, R_V is higher in the higher conditions for these low frequencies (Fig. 5C). Figure 5D shows a different frequency profile for conditions 1 and 2 compared to condition 3: For conditions 1 and 2 R_V is negative for very low frequencies (< 0.5Hz), positive for frequencies between 0.5 and 2 Hz, and then converges to 0 at higher frequencies. The frequency spectrum for condition 3

is largely opposite. The pattern of R_V at frequencies below 0.5 Hz largely corresponds to time-domain analysis shown in figure 4, which is expected since these low frequencies contain most power and thus largely determine the overall variance of the signals. The pattern of R_V for frequencies 0.5 – 2 Hz is the opposite showing the largest muscle synergy in condition 1 and 2 (R_V > 0), which is strongly diminished in condition 3. In frequencies above 2 Hz the effect reverses again and is similar to the effect seen in the lowest frequencies. ANOVA of R_V *(f)* showed significant effects of synergy level for frequencies below 0.5 Hz (F (2,30) = 75.79, p < 0.001), for frequencies between 0.5 and 2 Hz (F (1.4,21.3) = 8.13, p = 0.005) and for frequencies above 2 Hz (F (2,30) = 6.56, p = 0.004).

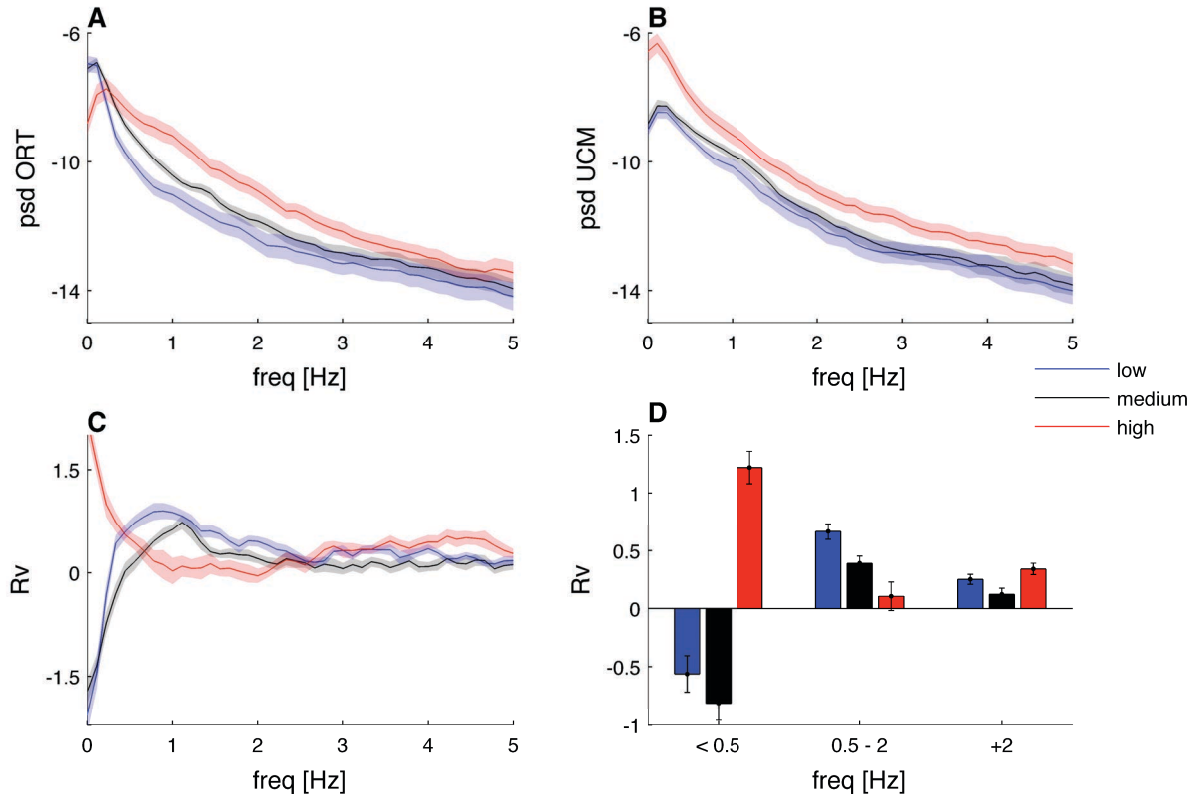

Figure 5. UCM analysis in frequency domain. The solid lines and bars represent grand averages, averaged over the 20 trials per synergy level and averaged over all participants. The shaded areas under the lines and the error bars in the bar graph represent the standard error of the mean. Each colour shows one of the three synergy levels (blue = low, black = medium, red = high). **A)** Power spectral density in the orthogonal dimension (psd ORT). **B)** Power spectral density in the uncontrolled manifold dimension (psd UCM). **C)** R_v in frequency domain. **D)** R_v divided in and averaged over three frequency bands, i.e.: (0-0.5 Hz, 0.5-2 Hz, 2-10 Hz). Note: psd ORT and psd UCM are log transformed before plotting.

To further investigate the frequency relationship between F_l and F_r we assessed the coherence and relative phase between both signals (Fig. 6). For condition 1 and 2 coherence was significant between 0 – 1.5 Hz. For condition 3, coherence was significant over the whole frequency range. When divided into the same frequency bands as R_V (Fig. 5D and 6B), ANOVA showed a significant main effect of synergy level (F (2,30) = 4.54, p = 0.019) and of frequency band (F (2,30) = 59.48, p < 0.001) and no significant interaction effect. The phase difference shows that in condition 1 and 2 bilateral forces have an anti-phase relationship (i.e. about π rad) for frequencies between 0 – 0.5 Hz,

while they have an in-phase relationship for frequencies between 0.5 – 2 Hz (i.e. about 0 or 2π rad). For frequencies above 2 Hz the phase relationship becomes less consistent. In contrast, in condition 3 the bilateral force signals were in phase for all frequencies. The effects seen in R_V (Fig. 5C and D) and in MSC (Fig. 6A and B) largely agree. The most obvious difference is the large negative values for R_V in conditions 1 and 2 in low frequencies (<0.5Hz), which is not directly reflected in the MSC, but this is explained by the clear anti-phase relationship in those conditions and frequency band (Fig. 6C), i.e. a consistent anti-phase relationship gives a negative R_V value.

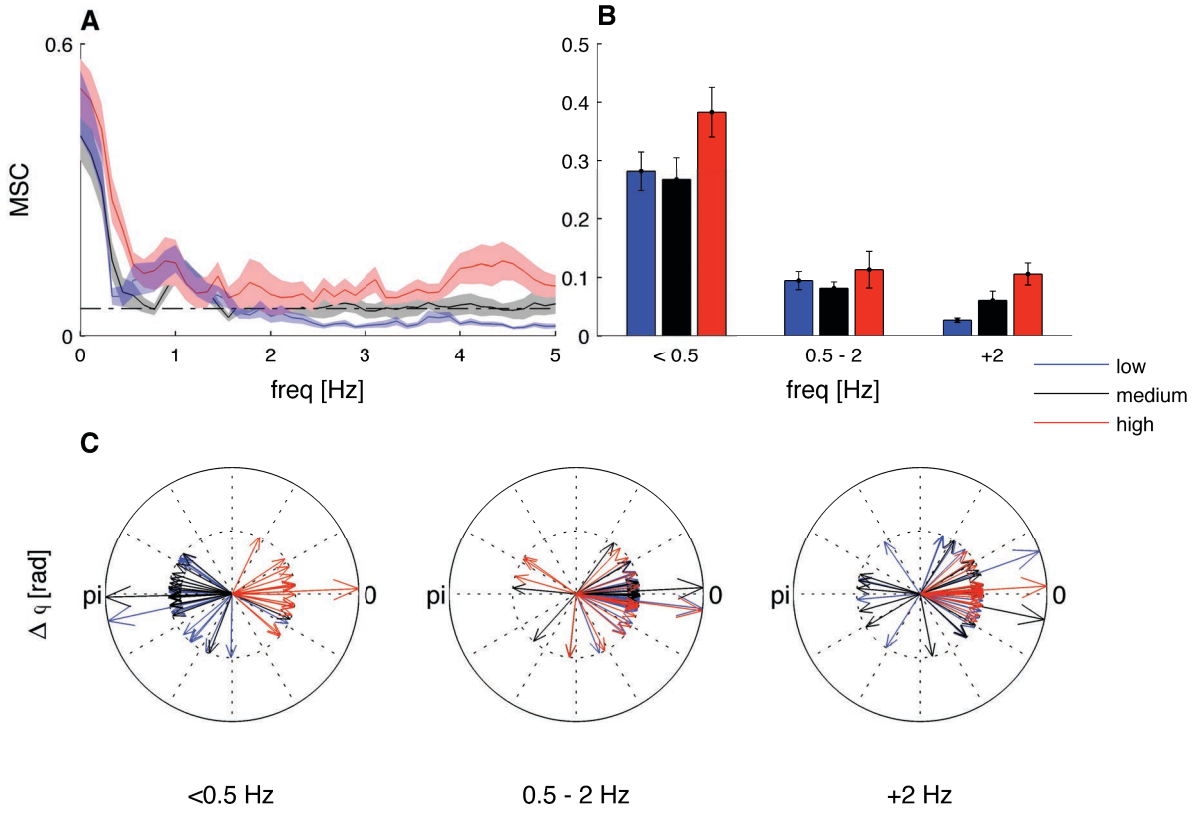

Figure 6. Coherence and relative phase between bilateral force signals. The solid lines and bars represent grand averages, averaged over the 20 trials per synergy level and averaged over all participants. The shaded areas under the lines and the error bars in the bar graph represent the standard error of the mean. Each colour shows one of the three synergy levels (blue = low synergy level, black = medium synergy level, red = high synergy level). **A)** Magnitude squared coherence between the two force signals (MSC). Dotted lines are the 95% confidence intervals for significant coherence. **B)** MSC divided in and averaged over three frequency bands, i.e.: (0-0.5 Hz, 0.5-2 Hz, 2-5 Hz). **C)** Relative phase between the two force signals ($\Delta\boldsymbol{\phi}$) divided in and averaged over the same three frequency bands as in **B**. Short arrows are individual participants, long arrows are grand averages.

3.2 Source Analysis

Using DICS we localized one source showing maximal CMC in the beta frequency range (23 ± 7 Hz) for each hand. Figure 7 shows the sources visualized on an MRI template (Holmes et al., 1998). The coordinates of the sources in the MNI coordinate system are [4.7, 0.5, 5.5] cm and [-4.2, 0.0, 6.0] cm

for the left and right hand, respectively. These sources are as expected in the contralateral motor cortex.

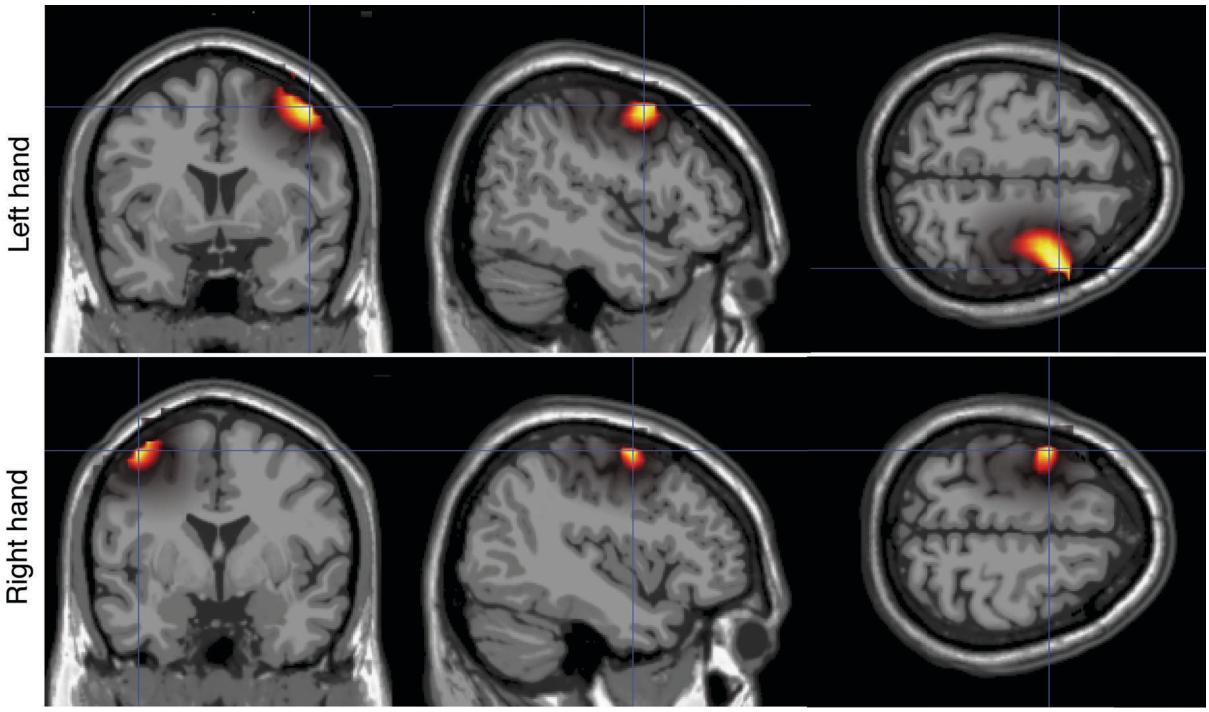

Figure 7. Sources of maximal CMC. Upper row shows the source with maximal CMC with the left hand EMG signal. Lower row shows the source with maximal CMC with the right hand EMG signal. Orthogonal blue lines intersect at the maximal CMC voxel. Sources are displayed on an MRI template.

3.3 CMC and IMC

To improve the estimation of common input, the leading 4 principal components were removed from the HDsEMG signals (left hand 3.6 ± 7.2, right hand 4.5 ± 6.0), and signals were reconstructed using the remaining PCs (van de Steeg et al., 2014). The reconstructed EMG signals were then rectified and averaged before coherence analysis.

As expected, CMC computed over the constant force interval was significant in the beta band (16-30 Hz; Fig. 8A). Beta-band coherence decreased with increasing synergy level for both absolute force levels and for both sides, except for CMC with left hand between synergy level 1 and 2 (Fig. 8B and C). In contrast, IMC was only significant in the alpha-band (5-12 Hz; Fig. 8A) and only in the high synergy condition. IMC in the alpha-band increased at higher synergy levels (Fig. 8B and C). ANOVA showed a significant main effect of synergy level for MSC for all three types of coherence, i.e.: CMC between left hand and right cortex (F (2,30) = 12.25, $p < 0.001$), CMC between right hand and left cortex (F (1.6,23.5) = 11.88, $p = 0.001$) and IMC between both hands (F (1.5,22.5) = 10.19, $p = 0.002$). There is no significant interaction effect and only a small decrease in CMC at higher absolute force levels between right hand and left cortex (F (1,15) = 7.09, $p = 0.018$) and a small decrease in IMC at higher force levels (F (1,15) = 5.15, $p = 0.038$).

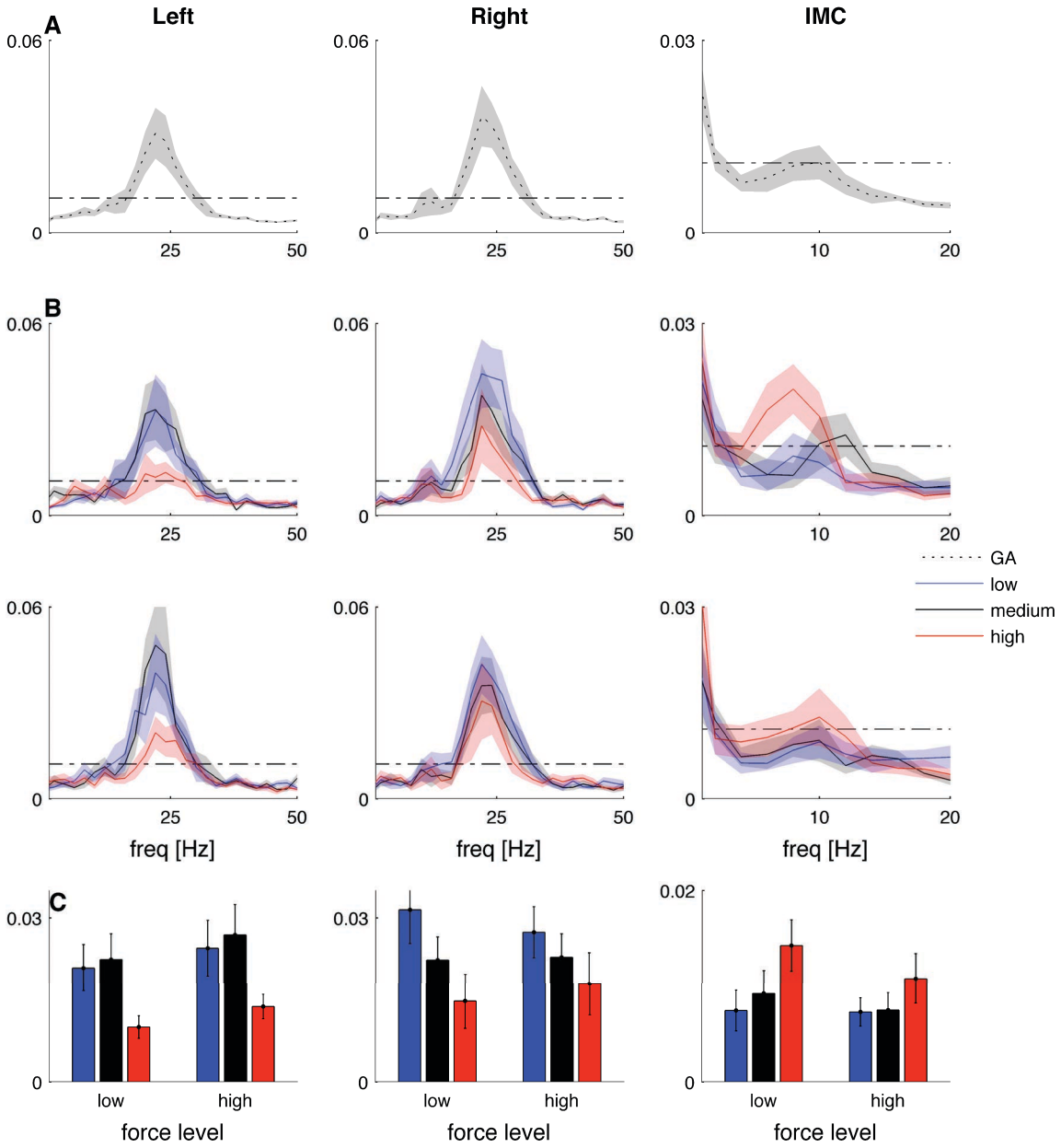

Figure 8. Magnitude squared coherence (MSC). Lines and bars are averages over participants, shaded areas and error bars in bar graphs are standard error of the mean and dash-dot lines are the 95% confidence interval for significant coherence. Columns depict from left to right: MSC between left hand and right motor cortex, MSC between right hand and left motor cortex and MSC between both hands. **A)** Grand Averages. **B)** Coherence spectra at the three synergy levels (blue = low synergy level, black = medium synergy level, red = high synergy level). The upper and lower row in **B** show absolute force level low and high, respectively. **C)** Averaged over significant frequency bands (16 – 30 Hz for CMC and 5 – 12 Hz for IMC). Colour coding is same as in **B**.

4. Discussion

In this study we investigated the neurophysiological mechanisms of muscle synergies using corticomuscular and intermuscular coherence. We experimentally manipulated the degree of muscle synergy and simultaneously measured brain activity (EEG) and muscle activity (HDsEMG). The results of our analysis of muscle synergies in the frequency domain suggest that there are three distinct

timescales at play in the emergence of muscle synergies. The results of the coherence analysis are in accordance with our hypothesis, i.e. with an increasing degree of muscle synergy corticomuscular coherence decreases whereas intermuscular coherence increases.

4.1 Muscle Synergies

We used the Uncontrolled Manifold (UCM) method to quantify the synergy between bilateral hand muscles, which showed that the manipulation had the intended effect. Hence, in the trials where a strong synergy was required, the variance within a trial was much larger in the dimension irrelevant for task success than in the dimension relevant for task success. In contrast, in the trials where a weak synergy was required, the variance was structured in the opposite direction (Fig. 4).

Scholz et al. (2003) found different timescales involved in the structure of variability. Their findings suggest that there is control on two hierarchical levels, i.e. a high level voluntary control that reduces the variance in the task-relevant dimension (V_{ORT}) on a larger timescale (> 250 ms), and a low level involuntary control that channels the variance into the task-irrelevant dimension (V_{UCM}) on a smaller timescale (< 250 ms). To test for a difference in timescales in bilateral synergies, we extended the UCM analysis to the frequency domain by using the power spectral density in the two dimensions (Fig. 5). Indeed, our results show a similar difference in the timescales of PSD_{ORT} and PSD_{UCM}, i.e. below 0.5 Hz PSD_{ORT} is smaller in the high synergy condition, whereas above 0.5 Hz there is an opposite effect. PSD_{UCM} is larger in the high synergy condition across all frequencies. This might indeed reflect that high-level voluntary control operates on slow timescales to minimize variance in the task-relevant dimension, whereas the larger variance in the uncontrolled manifold might reflect an involuntary error correction mechanism. The apparent difference in timescales between our findings and their findings (Scholz et al., 2003) reflects their choice of an arbitrary cut-off frequency of 4 Hz (i.e. 250 ms). By calculating R_V in the frequency domain there is no need to choose a priori an arbitrary cut-off frequency.

Our results for R_V in the frequency domain suggest that there are three different timescales at play (Fig. 5). In low frequencies (0 – 0.5 Hz) R_V is highest in the high synergy condition, whereas in frequencies roughly between 0.5 and 2 Hz this effect is largely the opposite. For frequencies higher than 2 Hz the effect switches again, i.e. R_V is highest in the high synergy condition. While the effects seen in the low and high frequency ranges (0 – 0.5 Hz and +2Hz) are as expected, the effect in the 0.5 to 2 Hz range is somewhat surprising. The higher variance in the task-relevant dimension in the high synergy condition may result from delays in feedback control. Visually guided responses have a feedback delay of about 200 – 300 ms, which accounts for oscillations in force signals with a period length of twice the delay time (i.e. 400 – 600 ms) when visually tracking a target force (Miall & Wolpert, 1996; Miall, 1996). In the high synergy condition each hand is tightly tracking the visual force signal produced by the other hand, and because of the visual feedback delay, there is always a small phase difference between the two forces. Indeed, our results of the coherence and relative phase analysis (Fig. 6) show that for the high synergy condition forces are in phase for most of the frequencies, except for 0.5 – 2 Hz where there is a small phase difference. This small phase difference may reflect the visual feedback delay and explains the lower R_V values in this frequency range. In contrast, the lower synergy conditions (1 and 2) required less tight coupling since the target *x*-position is much less sensitive to differences between the two force signals. These

conditions were perceived much easier for subjects and it was easier for the hands to track each other, resulting in smaller phase differences between forces (Fig. 6) and higher R_V values (Fig. 5).

4.2 CMC and IMC

CMC and IMC were significant in the beta (16-30 Hz) and alpha (5-12 Hz) frequency bands, respectively (Fig. 8). These frequency ranges are comparable with previous findings studying CMC and IMC in similar tasks (Baker et al., 1997; Boonstra, van Wijk, et al., 2009). There was a significant effect of synergy level both on CMC and IMC: CMC decreased and IMC increased at higher levels of bimanual synergy. These results are in agreement with the notion that corticomuscular and intermuscular coherence reflect two distinct neural pathways (Boonstra, van Wijk, et al., 2009) and support the hypothesis that neural motor control is divided in a phylogenetically older system containing descending projections driving spinal interneuronal modules and a phylogenetically newer system containing monosynaptic innervations to motoneurons of individual muscles (Bizzi & Cheung, 2013). The older pathway then diverges at the level of the spinal modules to innervate separate muscles coordinated with a common drive (i.e. muscle synergy) and results in intermuscular coherence. The newer pathway acts to further shape the activation of specific muscles, making it possible for higher primates and humans to control hand movements in a highly controlled manner. Depending on the required level of muscle synergy the contribution of both pathways is varied resulting in opposite changes in corticomuscular and intermuscular coherence.

An important issue that has been raised about studying muscle synergies is that it is difficult to distinguish low- and high-level interpretations of synergies, since in most studies the predicted synergies could be explained by appropriate hardwired circuits or biomechanical links (Valero-Cuevas, Venkadesan, & Todorov, 2009). The same goes for most studies investigating intermuscular coherence, i.e. they involve ipsilateral antagonist muscles often with direct anatomical connections or even motor units within a muscle (e.g. Bremner, Baker, & Stephens, 1991; Datta, Farmer, & Stephens, 1991; Fuglevand, 2011; Winges, Kornatz, & Santello, 2008). Nazarpour and colleagues tackled this problem by introducing abstract tasks where arbitrary muscle pairs have to coordinate (Nazarpour et al., 2012). They found that muscles that have no direct anatomical connection could rapidly form coordinated synergies if required by an abstract new task. They suggest that even if low-level anatomical synergies may be used, these can be readily overwritten and that the extensive divergence and convergence in the corticospinal system forms a substrate on which abstract task-dependent synergies emerge from optimization for high-level task requirements. In the current study, similar to Nazarpour et al. (2012) we avoid the problem of biomechanical links altogether by looking at bimanual homologous hand muscles. The bimanual muscle synergies studied here do not rule out a role of hardwired spinal interneuronal modules causing most of the coordination. However, the large task-dependent differences seen in both the behavioural data and the electrophysiological data suggest that even if there are low-level spinal modules involved, most of the coordination seen in our results comes from flexible high-level control policies.

4.3 Final Remarks

Our extension of the UCM analysis in the frequency domain suggests movement variability is not equally structured across timescales. It would be interesting to revisit some of the traditional experiments of the group of Latash and use the UCM analysis in the frequency domain to investigate all the different timescales that are involved.

The current findings provide us with a method to directly measure muscle synergies on a neurophysiological level (i.e. by combining intermuscular coherence with corticomuscular coherence). This can be used in clinical research in patients with diseases that prevent effective muscle synergies to occur, or diseases that show pathological synergies (e.g. stroke). If the problems in specific patient groups with muscle synergies are better understood in terms of the neurophysiology, it might help to develop more effective rehabilitation interventions (e.g. including electrophysiological stimulation).

The use of a volume conduction model, a source model and MRI based on templates for source analysis is not ideal and our analysis would benefit from using individual anatomical data, but if individual MRI is not available using templates is a good alternative.

5. Acknowledgements

All subjects: thank you for sacrificing some of your time and energy for my experiments. For the first few of you it took a bit longer than I promised, but you were all very patient.

Marjolein, Nick and Parinaz: thank you for your helpful hands with conducting the experiments. It would have been almost impossible to do everything by my self.

Dick: Bedankt voor je advies over HDsEMG en over de proefopstelling in het algemeen.

Bert Clairbois en Bert Coolen: bedankt voor al jullie hulp bij het verwezenlijken van de experimentele opzet. Als er iets fout ging met software of hardware op het laatste moment voor een meting, schoten jullie altijd snel en effectief te hulp.

Andreas: Bedankt voor je begeleiding en al je tips in de goede richting. Iedere keer als ik dacht dat ik ergens vastliep (vooral voor en tijdens de metingen) wuifde je mijn zorgen weg en verdwenen de problemen.

Tjeerd: Bedankt voor je intensieve begeleiding, vooral tijdens de data analyse in Sydney. Je verwelkomde me warm in het Black Dog Institute en zorgde er voor dat ik nergens te lang vast zat tijdens de analyse. Verder, bedankt voor al je nuttige en uitgebreide commentaar op alle versies van mijn onderzoeksvoorstel en van deze thesis.

Pap, mam en Jesse: bedankt voor jullie onvoorwaardelijke liefde en steun tijdens mijn hele studie. Als ik met mezelf in de knoop zat kon ik altijd op jullie steun rekenen. Mam, je las ieder stuk dat ik schreef en gaf altijd uitgebreid en nuttig commentaar, bedankt!

Lola: Thank you for your love and support. Volim te, knedlice.

6. References

Baker, S. N., Olivier, E., & Lemon, R. N. (1997). EMG show task-dependent modulation. *Journal of Physiology*, *501*(1), 225–241.

Bernstein, N. (1967). *The Co-ordination and regulation of movements*.

Bizzi, E., & Cheung, V. C. K. (2013). The neural origin of muscle synergies. *Frontiers in Computational Neuroscience*, *7*(April), 51. doi:10.3389/fncom.2013.00051

Boonstra, T. W., & Breakspear, M. (2012). Neural mechanisms of intermuscular coherence: implications for the rectification of surface electromyography. *Journal of Neurophysiology*, *107*(3), 796–807. doi:10.1152/jn.00066.2011

Boonstra, T. W., Clairbois, H. E., Daffertshofer, A., Verbunt, J., van Dijk, B. W., & Beek, P. J. (2005). MEG-compatible force sensor. *Journal of Neuroscience Methods*, *144*(2), 193–6. doi:10.1016/j.jneumeth.2004.11.004

Boonstra, T. W., Daffertshofer, A., Roerdink, M., Flipse, I., Groenewoud, K., & Beek, P. J. (2009). Bilateral motor unit synchronization of leg muscles during a simple dynamic balance task. *The European Journal of Neuroscience*, *29*(3), 613–22. doi:10.1111/j.1460-9568.2008.06584.x

Boonstra, T. W., van Wijk, B. C. M., Praamstra, P., & Daffertshofer, A. (2009). Corticomuscular and bilateral EMG coherence reflect distinct aspects of neural synchronization. *Neuroscience Letters*, *463*(1), 17–21. doi:10.1016/j.neulet.2009.07.043

Bremner, F., Baker, J., & Stephens, J. (1991). Variation in the degree of synchronization exhibited by motor units lying in different finger muscles in man. *The Journal of Physiology*, *432*(1), 381–399. Retrieved from http://jp.physoc.org/content/432/1/381.short

Bruns, A. (2004). Fourier-, Hilbert- and wavelet-based signal analysis: are they really different approaches? *Journal of Neuroscience Methods*, *137*(2), 321–32. doi:10.1016/j.jneumeth.2004.03.002

Datta, B. Y. A. K., Farmer, S. F., & Stephens, J. A. (1991). Central nervous pathways underlying synchronization of human MU firing studied during voluntary contraction. *The Journal of Physiology*, *432*, 401–425.

Diedrichsen, J., Shadmehr, R., & Ivry, R. B. (2010). The coordination of movement: optimal feedback control and beyond. *Trends in Cognitive Sciences*, *14*(1), 31–9. doi:10.1016/j.tics.2009.11.004

Farina, D., Negro, F., & Jiang, N. (2013). Identification of common synaptic inputs to motor neurons from the rectified electromyogram. *The Journal of Physiology*, *591*(Pt 10), 2403–18. doi:10.1113/jphysiol.2012.246082

Fuglevand, A. J. (2011). Mechanical properties and neural control of human hand motor units. *The Journal of Physiology*, *589*(Pt 23), 5595–602. doi:10.1113/jphysiol.2011.215236

Gross, J., Kujala, J., Ha, M., Timmermann, L., Schnitzler, A., & Salmelin, R. (2001). Dynamic imaging of coherent sources : Studying neural interactions in the human brain, *98*(2).

Holmes, C., Hoge, R., Collins, L., Woods, R., Toga, A., & AC, E. (1998). Enhancement of MR images using registration for signal averaging. *J Comput Assist Tomogr*, *22*(2), 324–333.

Jung, T.-P., Makeig, S., Humphries, C., Lee, T.-W., McKeown, M. J., Iragui, V., & Sejnowski, T. J. (2000). Removing electroencephalographic artifacts by blind source separation. *Psychophysiology*, *37*(2), 163–178. doi:10.1111/1469-8986.3720163

Kelso, J. (2008). *Synergies*. *Scholarpedia*. doi:10.4249/scholarpedia.1611

Latash, M., Scholz, J., & Schöner, G. (2002). Motor control strategies revealed in the structure of motor variability. *Exercise and Sport Sciences …*, *30*(1), 26–31. Retrieved from http://www.ncbi.nlm.nih.gov/pubmed/11800496

Latash, M., Scholz, J., & Schöner, G. (2007). Toward a new theory of motor synergies. *Motor Control*, *11*(3), 276–308. Retrieved from http://www.ncbi.nlm.nih.gov/pubmed/17715460

Miall, R. C. (1996). Task-dependent changes in visual feedback control: a frequency analysis of human manual tracking. *Journal of Motor Behavior*, *28*(2), 125–35. doi:10.1080/00222895.1996.9941739

Miall, R. C., & Wolpert, D. M. (1996). Forward Models for Physiological Motor Control. *Neural Networks : The Official Journal of the International Neural Network Society*, *9*(8), 1265–1279. Retrieved from http://www.ncbi.nlm.nih.gov/pubmed/12662535

Mitra, P. P., & Pesaran, B. (1999). Analysis of dynamic brain imaging data. *Biophysical Journal*, *76*(2), 691–708. doi:10.1016/S0006-3495(99)77236-X

Myers, L. ., Lowery, M., O'Malley, M., Vaughan, C. ., Heneghan, C., St Clair Gibson, A., … Sreenivasan, R. (2003). Rectification and non-linear pre-processing of EMG signals for cortico-muscular analysis. *Journal of Neuroscience Methods*, *124*(2), 157–165. doi:10.1016/S0165-0270(03)00004-9

Nazarpour, K., Barnard, A., & Jackson, A. (2012). Flexible cortical control of task-specific muscle synergies. *The Journal of Neuroscience : The Official Journal of the Society for Neuroscience*, *32*(36), 12349–60. doi:10.1523/JNEUROSCI.5481-11.2012

Oostenveld, R., Fries, P., Maris, E., & Schoffelen, J. M. (2011). FieldTrip: Open source software for advanced analysis of MEG, EEG, and invasive electrophysiological data. *Computational Intelligence and Neuroscience*, *2011*, 156869. doi:10.1155/2011/156869

Oostenveld, R., Stegeman, D. F., Praamstra, P., & Oosterom, A. (2003). Brain symmetry and topographic analysis of lateralized event-related potentials. *Clinical Neurophysiology*, *114*(7), 1194–1202.

Rosenberg, J., Amjad, A., Breeze, P., Brillinger, D., & Halliday, D. (1989). The Fourier approach to the identification of functional coupling between neuronal spike trains. *Progress in Biophysics …*, *53*(1980), 1–31. Retrieved from http://scholar.google.com/scholar?hl=en&btnG=Search&q=intitle:The+fourier+approach+to+identification+of+coupling+between+neuronal+spike+trains.#0

Schoffelen, J., Poort, J., Oostenveld, R., & Fries, P. (2011). Selective Movement Preparation Is Subserved by Selective Increases in Corticomuscular Gamma-Band Coherence, *31*(18), 6750–6758. doi:10.1523/JNEUROSCI.4882-10.2011

Scholz, J. P., Kang, N., Patterson, D., & Latash, M. L. (2003). Uncontrolled manifold analysis of single trials during multi-finger force production by persons with and without Down syndrome. *Experimental Brain Research*, *153*(1), 45–58. doi:10.1007/s00221-003-1580-8

Scott, S. H. (2004). Optimal feedback control and the neural basis of volitional motor control. *Nature Reviews. Neuroscience*, *5*(7), 532–46. doi:10.1038/nrn1427

Staudenmann, D., Kingma, I., Daffertshofer, A., Stegeman, D. F., & van Dieën, J. H. (2006). Improving EMG-based muscle force estimation by using a high-density EMG grid and principal component analysis. *IEEE Transactions on Bio-Medical Engineering*, *53*(4), 712–9. doi:10.1109/TBME.2006.870246

Ting, L. H., Chvatal, S. A., Safavynia, S. A., & Mckay, J. L. (2012). Review and perspective : neuromechanical considerations for predicting muscle activation patterns for movement. *Internation Journal for Numerical Methods in Biomedical Engineering*, *28*(May), 1003–1014. doi:10.1002/cnm

Ting, L. H., & McKay, J. L. (2007). Neuromechanics of muscle synergies for posture and movement. *Current Opinion in Neurobiology*, *17*(6), 622–8. doi:10.1016/j.conb.2008.01.002

Todorov, E. (2004). Optimality principles in sensorimotor control. *Nature Neuroscience*, *7*(9), 907–15. doi:10.1038/nn1309

Tuller, B., Turvey, M., & Fitch, H. (1982). The Bernstein perspective: II. The concept of muscle linkage or coordinative structure. In *Human motor behavior: An introduction* (pp. 253–270).

Turvey, M., Fitch, H., & Tuller, B. (1982). The Bernstein perspective: I. The problems of degrees of freedom and context-conditioned variability. In *Human motor behavior: An introduction* (pp. 239–252).

Valero-Cuevas, F. J., Venkadesan, M., & Todorov, E. (2009). Structured variability of muscle activations supports the minimal intervention principle of motor control. *Journal of Neurophysiology*, *102*(1), 59–68. doi:10.1152/jn.90324.2008

Van de Steeg, C., Daffertshofer, A., Stegeman, D. F., & Boonstra, T. W. (2014). High-density surface electromyography improves the identification of oscillatory synaptic inputs to motoneurons. *Journal of Applied Physiology (Bethesda, Md. : 1985)*, *116*(10), 1263–71. doi:10.1152/japplphysiol.01092.2013

Van Wijk, B. C. M., Beek, P. J., & Daffertshofer, A. (2012). Neural synchrony within the motor system: what have we learned so far? *Frontiers in Human Neuroscience*, *6*(September), 252. doi:10.3389/fnhum.2012.00252

Vereijken, B., Emmerik, R. E. A. van, Whiting, H. T. A., & Newell, K. M. (1992). Free(z)ing Degrees of Freedom in Skill Acquisition. *Journal of Motor Behavior*, *24*(1), 133–142. doi:10.1080/00222895.1992.9941608

Verrel, J. (2010). Distributional properties and variance-stabilizing transformations for measures of uncontrolled manifold effects. *Journal of Neuroscience Methods*, *191*(2), 166–70. doi:10.1016/j.jneumeth.2010.06.016

Winges, S. a, Kornatz, K. W., & Santello, M. (2008). Common input to motor units of intrinsic and extrinsic hand muscles during two-digit object hold. *Journal of Neurophysiology*, *99*(3), 1119–26. doi:10.1152/jn.01059.2007